JACS
JOURNAL OF THE AMERICAN CHEMICAL SOCIETY

pubs.acs.org/JACS

Article

How Do Local Reactivity Descriptors Shape the Potential Energy Surface Associated with Chemical Reactions? The Valence Bond Delocalization Perspective

Thijs Stuyver,* Frank De Proft, Paul Geerlings, and Sason Shaik*

Cite This: *J. Am. Chem. Soc.* 2020, 142, 10102−10113

Read Online

ACCESS | Metrics & More | Article Recommendations | Supporting Information

ABSTRACT: How do local reactivity descriptors, such as the Fukui function and the local spin density distribution, shape the potential energy surface (PES) associated with chemical reactions and thus govern reactivity trends and regioselective preferences? This is the question that is addressed here through a qualitative valence bond (VB) analysis. We demonstrate that common density functional theory (DFT)-based local reactivity descriptors can essentially be regarded—in one way or another—as indirect measures of delocalization, i.e., resonance stabilization, of the reactants within VB theory. The inherent connection between (spatial) delocalization and (energetic) resonance stabilization embedded in VB theory provides a natural and elegant framework for analyzing and comprehending the impact of individual local reactivity descriptors on the global PES. Our analysis provides new insights into the role played by local reactivity descriptors and illustrates under which conditions they can sometimes fail to predict reactivity trends and regioselective preferences, e.g., in the case of ambident reactivity. This treatment constitutes *a first step toward a unification of VB theory and conceptual DFT*.

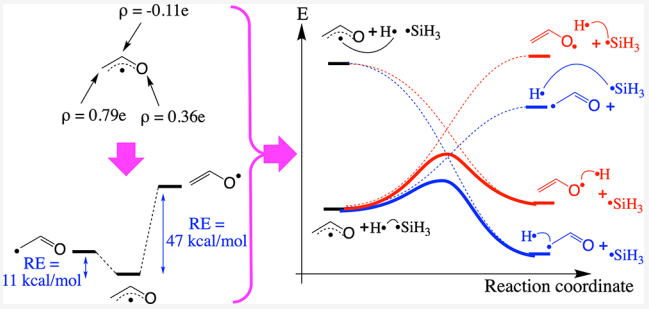

INTRODUCTION

Local reactivity descriptors, e.g., the Fukui function, the local softness, and the local spin density distribution, play a central role within the field of theoretical chemistry, and particularly within conceptual density functional theory (CDFT), as convenient and powerful tools to infer reactivity trends and regioselective preferences.[1−6] A vast literature has emerged around this topic in recent decades, and countless chemical systems have been identified for which a local reactivity descriptor approach provides an insightful framework for analysis.[7−10] Next to the many successes, however, a couple of problematic cases have been identified as well, for which the local reactivity descriptors fail to reproduce the reactivity trends/regioselective preference observed experimentally, e.g., ambident reactivity.[11−13]

Many reactivity descriptors, especially those originating from CDFT, emerge from a perturbational approach; i.e., they are initial response properties of the considered chemical system under perturbations caused by the approach of a second reactant.[1] For example, the Fukui function corresponds to the response of the electron density of the chemical system to a change in the number of electrons, i.e., to electron transfer. Depending on whether an electron is added to, or removed from, the chemical system under consideration, one effectively ends up with the densities associated with the highest occupied and/or lowest unoccupied molecular orbitals (HOMOs and LUMOs, which are also the central entities of interest in frontier molecular orbital theory).[14] It has been amply demonstrated that consideration of the atom-condensed Fukui function values for a chemical system enables the identification of the site(s) most prone to either electrophilic or nucleophilic attack.[1−3] In a similar way, the magnitudes of atom-condensed spin densities have recently been connected phenomenologically to the tendency of (di/poly)radical compounds to take part in radical reactions.[6]

Since all (local) reactivity descriptors are essentially properties of (one of) the isolated reaction partners, the observation that they enable prediction of reaction pathway preferences implies that, somehow, *these properties shape the potential energy surfaces (PESs) associated with the respective competing reaction pathways across the entire reaction coordinate in a decisive way*.

Even though the latter statement is an obvious prerequisite for a reactivity descriptor to have any predictive power, the exact mechanism through which the descriptors mentioned above impact the overall PES has received comparatively little attention so far. As already indicated, many reactivity

Received: March 1, 2020
Published: May 5, 2020

https://dx.doi.org/10.1021/jacs.0c02390
J. Am. Chem. Soc. 2020, 142, 10102−10113

descriptors have been cast within CDFT theory as measures which enable us to identify the reaction pathway which—at the onset of the reaction—provides the optimal energetic response of the system. But, does this initial response trend necessarily persist throughout the entire reaction? Additionally, to what extent do these individual descriptors impact the kinetics, i.e., the reaction barriers, versus the thermodynamic driving forces, i.e., the endo-/exothermicity, associated with the different competing reaction pathways?

To the best of our knowledge, these are outstanding issues which have not yet been addressed in a clear and conclusive way. In fact, it is worth mentioning here that the broader kinetics vs thermodynamics conundrum, associated with local reactivity descriptors, figured prominently as one of the "issues of reflection concerning the future of CDFT", identified during a recent round-table discussion among leading experts within the CDFT field; cf. ref 3. As such, in the present contribution, we address the following questions: how do the properties of the reactants impact the PES of their particular reaction, and to what extent can local reactivity descriptors be trusted to accurately discriminate between different reaction pathways and identify the most favorable one?

To this end, we turn to qualitative valence bond (VB) theory, which enables the lucid and insightful description of the shape of the PES associated with a reaction.[15−19] As we demonstrate below, many common local reactivity descriptors can essentially be regarded within VB theory—in one way or another—as indirect measures of delocalization, i.e., resonance stabilization, of the reactants. The inherent connection between (spatial) delocalization and (energetic) resonance stabilization embedded in this theory provides a natural and elegant framework through which the impact of individual local reactivity descriptors on the global PES can be analyzed and understood. As such, our analysis constitutes a first step toward an eventual unification of VB theory and CDFT.[20]

Initially, we focus mainly on the role of the spin density distribution on radical reactions. Subsequently, we discuss briefly the role played by the Fukui function in nucleophilic/electrophilic reactions. Overall, our analysis provides new insights into the role played by local reactivity descriptors and illustrates under which conditions they can sometimes fail to predict reactivity trends and regioselective preferences.

COMPUTATIONAL DETAILS

Geometry optimizations of the various species were carried out at the (U)B3LYP/cc-pVTZ[21] level of theory with the help of the Gaussian09 program (the 6-311++G** basis set was tested as well and gave almost identical results; cf. Section S2 in the Supporting Information).[22] Atomic charges and (condensed) spin density distributions were determined from a natural population (NBO) analysis.[23] Atom-condensed Fukui function (f^-) amplitudes for a vinyloxy anion were determined by subtracting the atom-condensed NBO electron densities for the uncharged species, i.e., vinyloxy anion from which one electron has been removed, from the corresponding densities obtained for the original anionic species (cf. eq 3 below).

All VB calculations were carried out with the XMVB software package[24] at the VBSCF level of theory with a 6-311++G** basis set on the optimized geometries resulting from the Gaussian09 calculations. Due to the planarity of the molecules, the π- and σ-systems could be separated, enabling the VB procedure to be effectively limited to the π-atomic orbitals (the σ-system was treated as frozen MO orbitals).[25] For each of the considered molecules, the VB structures were constructed from hybrid atomic orbitals (HAOs), and both ionic and covalent structures were explicitly taken into account.[15] The energies associated with specific adiabatic states were determined in separate VBSCF calculations involving the corresponding subset of structures contributing to this state.[15]

RESULTS AND DISCUSSION

Qualitative Valence Bond Theory. Let us start by introducing some elementary notions concerning qualitative valence bond (VB) theory. As indicated in the Introduction, qualitative VB analysis involves the construction of VB reactivity diagrams which reflect the shape of the PES associated with a given chemical system along a chosen reaction coordinate. Usually, one starts by examining the evolution of the so-called "diabatic curves", which represent the wave function associated with a limited number of VB structures; i.e., they correspond to a localized VB configuration (e.g., a specific Lewis structure of the reactants or products). These individual diabatic curves interact along the reaction coordinate, and collectively they give rise to the "adiabatic" curve, i.e., the full ground-state PES associated with the chemical system under consideration (*vide infra*).

A comprehensive guide on the systematic construction of VB diagrams for the treatment of chemical reactivity problems can be found in Chapter 6 of ref 15. An alternative introduction to this topic can be found in the recent tutorial in ref 18. Here we present a concise overview of the main features of such diagrams, using a simple (and well-described)[6] model reaction: the (radical) hydrogen abstraction reaction between $H_3C^\bullet$ and H-SiH_3 (cf. Figure 1).

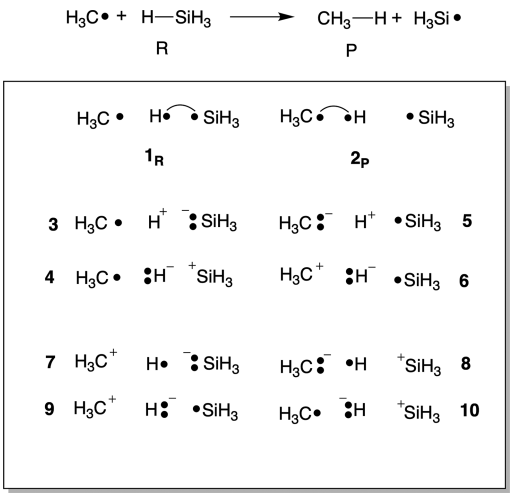

Figure 1. VB structure set contributing to the state wave function throughout the H-abstraction reaction. $\mathbf{1}_R$ and $\mathbf{2}_P$ are the covalent or Heitler−London (HL) structures describing the H−SiH_3 bond in the reactant (R) and the H−CH_3 bond in the product (P), respectively. The remaining structures (**3**−**10**) are ionic and charge-transfer (CT) structures, which mix into the wave function to a variable extent throughout the transformation.

The first step toward the construction of a VB diagram involves the plotting of the diabatic energy curves corresponding to the electronic structure of the reactants and products for the considered reaction as a function of the reaction coordinate. For the simple model reaction considered here, the H−SiH_3 bond in the reactant (R) and the H−CH_3 bond in the product (P) can—in the first instance—be approximated respectively by the Heitler−London (HL) VB structures $\mathbf{1}_R$ and $\mathbf{2}_P$, wherein the arched lines connecting the electrons signify singlet electron pairing. By definition, the optimal

https://dx.doi.org/10.1021/jacs.0c02390
J. Am. Chem. Soc. 2020, 142, 10102−10113

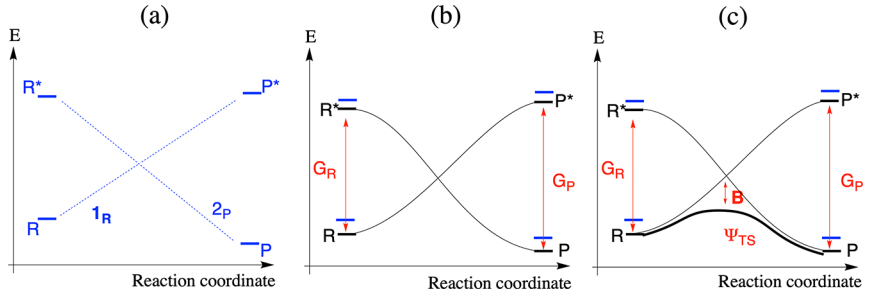

Figure 2. VB reactivity diagrams, depicting the diabatic and adiabatic energy curves along the reaction coordinate connecting the reactants (R), i.e., $H_3C^{\bullet}$ and H-SiH_3, to the products (P), i.e., H_3C−H and $^{\bullet}SiH_3$. (a) The HL structures (i.e., $\mathbf{1}_R$ and $\mathbf{2}_P$) are a first-order approximation of the electronic structures of R and P (as well as their excited analogues R* and P*) for the considered reaction. (b) The same VB diagram but now with the (secondary) ionic structures mixed into the diabatic reactant and product states (indicated by a change of color of the curves). This mixing leads to a stabilization of each of the considered species: the bold black lines, associated with the full electronic structures of R, P, R*, and P*, respectively, are all lower in energy than the corresponding bold blue lines, associated with the energy levels of the individual HL structures $\mathbf{1}_R$ and $\mathbf{2}_P$. G_R and G_P denote the promotion energies on the reactant and product side, respectively. (c) The same VB diagram but now with the adiabatic curve, arising from the mixing of the individual diabatic curves, included in bold. Ψ_{TS} denotes the transition state, and *B* corresponds to the resonance interaction between the two curves in the TS geometry.

reactant geometry is the geometry stabilizing structure $\mathbf{1}_R$ the most, whereas the optimal product geometry is the one stabilizing structure $\mathbf{2}_P$ the most. These two limiting geometries are connected through the reaction coordinate. As one proceeds from the optimal reactant geometry toward the optimal product geometry, $\mathbf{1}_R$ will rise in energy (due to Si−H bond dissociation while creating C−H Pauli repulsion). At the optimal product geometry, $\mathbf{1}_R$ can be considered as an approximation to the promoted—or excited—state of the product P, which is usually denoted by P*. Equivalently, $\mathbf{2}_P$ will also rise in energy as one moves away from the optimal product geometry, and, at the optimal reactant geometry, this VB structure can be considered as an approximation of the promoted state of the reactant R, denoted by R*. In this way, one has obtained the rudimentary shape of two crossing diabatic energy curves in a simple valence bond state correlation diagram (VBSCD), cf. Figure 2a.

So far, we have limited our discussion to the main HL structures. As evident from Figure 1, other (secondary) VB structures can be defined as well, namely the ionic and CT states. These structures mix with the $\mathbf{1}_R$ and $\mathbf{2}_P$ structures along the reaction coordinate. Let us first consider the effect of mixing in the ionic structures. Ionic structures **3** and **4** contribute to the H−SiH_3 Lewis bond in $\mathbf{1}_R$, while **5** and **6** contribute to the full Lewis bond in $\mathbf{2}_P$. Often, these ionic structures are directly combined with the HL structures to form the so-called diabatic reactant and product Lewis states, offering a more accurate description of R, R*, P, and P*, respectively (Figure 2b).

In the case that structures $\mathbf{1}_R$ and $\mathbf{2}_P$ provide a reasonably accurate description of the reactant and product electronic structure respectively (as they do for the model reaction considered here), the correction to the energy provided by mixing in these secondary VB structures (also called the covalent-ionic resonance energy) is rather small, so that the overall shape of the crossing curves is preserved. However, as we will discuss below, in the case that a single structure cannot describe the full wave function accurately, i.e., in the case of extensively delocalized species, the resonance energy can be quite significant, and fluctuations in this quantity along the reaction coordinate will directly affect the curvature of the PES (*vide infra*).

At this point, we would like to note that the fact that $\mathbf{1}_R$ and $\mathbf{2}_P$ are good descriptors of R and P is reflected in the respective spin density distributions. Thus, in both the reactant and product, our calculations indicate that the radical electrons are almost perfectly localized in both the reactant and the product, i.e., the NBO spin density on respectively the C- and Si-center approaches unity: $\rho(C) = 1.08e$ and $\rho(Si) = 0.97e$.

As explained in refs 15 and 16, the promotion energies, G_R and G_P, required to excite R to R* and P to P*, can be expressed as the singlet−triplet excitation energy of respectively the active reactant and product bond (H−SiH_3/H−CH_3). These quantities correspond approximately to twice the respective bond energies.[15] This promotion energy, together with the thermodynamic driving force (ΔE_{rp}), determines the height of the crossing point between the two energy curves. The following universal expression for the approximate height of this crossing point has previously been derived by Shaik et al.,[17]

$$E_{\text{crossing}} = f_0 G_0 + 0.5\Delta E_{rp} \quad (1)$$

where $f_0 G_0$ corresponds to a fraction (f_0) of the average of the promotion gap on the reactant and product sides,

$$G_0 = 0.5(G_R + G_P) \quad (2)$$

Once the energy curves corresponding to the full diabatic reactant and product states have been constructed, one proceeds to consider the interaction between the individual diabatic states and to complete thereby the shape of the adiabatic energy curve. At the optimal reactant geometry, the adiabatic energy curve coincides with the diabatic curve R (R* does not contribute to the wave function in this geometry), and equivalently, at the optimal product geometry, the adiabatic curve coincides with the diabatic curve P. However, at the crossing point between the two diabatic energy curves (corresponding to the transition state (TS) geometry), the reactant and product states mix significantly, pushing the adiabatic energy curve below the crossing point and leading to an avoided crossing in the VBSCD.

So far, we have not discussed structures **7**−**10** in Figure 2. These structures correspond to CT states because they involve an odd number of electrons in both the right-hand and left-hand bonds. At the optimal reactant or product geometries, **7**−**10** generally do not mix with the main structures $\mathbf{1}_R$ and $\mathbf{2}_P$, so

https://dx.doi.org/10.1021/jacs.0c02390
J. Am. Chem. Soc. 2020, 142, 10102−10113

they do not contribute to the reactant and product diabatic states. However, this mixing does become allowed in the region around the TS geometry (cf. Figure 2b). As such, inclusion of the CT states in the VB diagram pushes the adiabatic curve even further down in energy in this region. The final energy hill obtained, after taking all the mixing between the individual diabatic states into account, corresponds to the observed barrier of the chemical reaction (Figure 2c). The total amount of resonance stabilization of the transition state compared to the crossing point between reactant and product state is generally denoted by B.

By adding this B-factor, one can amend eq 1 to yield an expression for the approximate barrier height associated with a generic chemical reaction,

$$\Delta E^{\ddagger} = f_0 G_0 + 0.5\Delta E_{rp} - B \quad (3)$$

Let us now apply this equation to estimate the activation energy associated with the specific reaction we have taken as a model throughout this analysis, i.e., the H-abstraction reaction between $H_3C^{\bullet}$ and $H-SiH_3$. Using the previously determined properties of the curves for hydrogen abstraction reactions involving hydrocarbons, f_0 amounts approximately to 0.348, and B to 50 kcal/mol.[15,26,27] For $H-SiH_3$, the experimental BDE amounts to 87 kcal/mol, and for $H-CH_3$, this quantity amounts to 105 kcal/mol. As such, the averaged promotion gap G_0 can be crudely estimated to amount to 192 kcal/mol. Furthermore, since the overall effect of the hydrogen exchange reaction under consideration is the breaking of a Si−H bond and the formation of a C−H bond, the thermodynamic driving force ΔE_{rp} can be approximated as the energy difference between the two corresponding BDE values, i.e., $\Delta E_{rp} \approx -18$ kcal/mol. Inserting all these quantities into eq 3 leads to an estimated activation energy for the reaction of approximately 7.8 kcal/mol.

Calculation of the PES at UB3LYP/cc-pVTZ level of theory (with ZPE correction included) leads to an actual reaction barrier of 6.9 kcal/mol and a thermodynamic driving force of −13.4 kcal/mol. As such, these computed values agree within a reasonable margin with the crudely estimated ones, illustrating the usefulness of the VB model outlined above.

How Does Delocalization Affect the VBSCD Curve Shapes? In the previous section, we described a model reaction which involves a localized radical electron, so that both the reactant and product state could be approximated initially by a single (HL) structure. Let us now consider what happens to the shape of the PES when extensive delocalization enters the picture.

We focus again on a model: the hydrogen exchange reaction between allyl radical and SiH_4. It should be clear that a reaction between these two reagents can give rise to several reaction products. For the sake of the argument that follows, let us focus specifically on the products shown in Figure 3 (**P1** and **P2**), which are the most likely ones to arise. Obviously, these two products are chemically equivalent, but mathematically (when one assigns a uniform set of labels to the individual C-atoms), or if one ethylenic carbon is ^{14}C, their electronic structure is described distinctively.

Contrary to the localized (radical) system from the previous section, it is now impossible to define a single VB structure that represents the reactant state: the wave function associated with the allyl radical inherently consists of a linear combination of two equivalent Lewis VB structures (Figure 4a). The extent

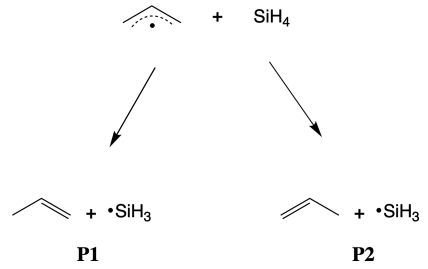

Figure 3. Some potential products formed from the reaction between allyl$^{\bullet}$ and SiH_4. The "+" signs indicate that the species on opposite sides of this sign do not interact; i.e., they are perfectly separated.

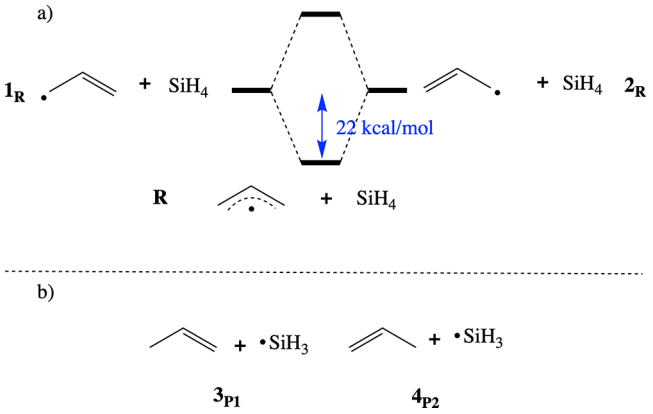

Figure 4. (a) Resonance mixing of the two localized structures and the resulting delocalized allyl radical. The displayed resonance energy was calculated at the VBSCF/6-311++G** level of theory. (b) Some relevant covalent VB structures associated with the products of the reaction between allyl radical and silane.

of mixing of the two equivalent localized structures taking part in the total wave function is significant; quantitative VB calculations at the VBSCF/6-311++G** level of theory point to an overall resonance stabilization of approximately 22 kcal/mol for the full wave function compared to its localized constituents (cf. Computational Details). As a consequence of the delocalized nature of the allyl radical, the atom-condensed spin density on neither of the extremal carbon centers of the allyl radical approaches unity; they both amount to 0.63e instead (with the central carbon center carrying a negative spin density of −0.27e; for a VB analysis of the origins of the negative spin density on the central carbon atom, see page 216 in ref 15). The individual products, on the other hand, can be perfectly described by a single (Lewis) VB structure each (Figure 4b). As a consequence, the radical centers for these species are perfectly localized: the NBO spin density on the Si-atom approaches unity (ρ(Si) = 0.97e).

Note that the fact that $\mathbf{3_{P1}}$ best describes the first product in Figure 3 (**P1**) does not mean that the other product VB structure does not formally partake in the wave function associated with **P1**: $\mathbf{4_{P2}}$ will nominally contribute to the full electronic structure of this first product as well, but its weight will essentially be zero since it can be expected to be much higher in energy than $\mathbf{3_{P1}}$ in this geometry, and the resonance energy it provides will be negligible (Figure 5). The exact same reasoning applies to the second product in Figure 3 (**P2**).

As such, one can conclude that the resonance energy associated with the delocalization of the radical electron which

https://dx.doi.org/10.1021/jacs.0c02390
J. Am. Chem. Soc. 2020, 142, 10102−10113

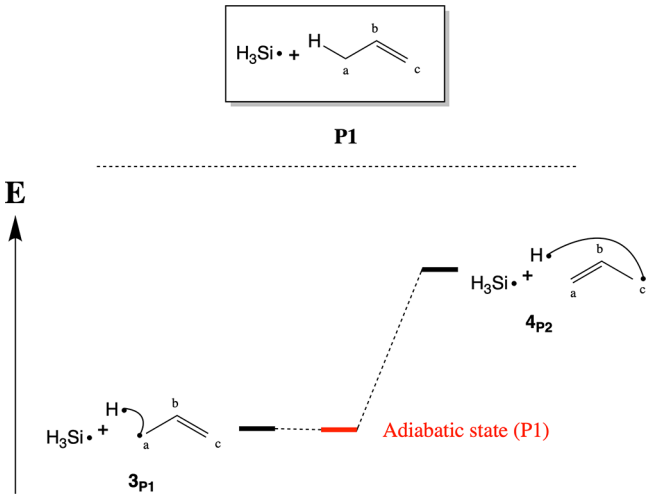

Figure 5. Geometry of product **P1** (top) and the valence bond mixing diagram of $\mathbf{3}_{P1}$ and $\mathbf{4}_{P2}$ which generates this product (bottom). In the **P1** geometry, VB structure $\mathbf{3}_{P1}$ is much lower in energy than structure $\mathbf{4}_{P2}$. Consequently, $\mathbf{4}_{P2}$ only contributes formally to the adiabatic ground state of **P1**; the mixing between the two structures is essentially zero, giving rise to an adiabatic state **P1** (shown in red) that consists more or less exclusively of structure $\mathbf{3}_{P1}$.

is present in the reactant is lost once either of the possible products is reached.

Note that the impact of the loss of delocalization is reflected in both the evolution of the spin density distribution throughout the reaction and the geometry of the system. Whereas in the reactant allyl radical the two C−C bonds are equal in length due to the resonance between the two individual localized VB structures, the product propene has two unequal C−C bonds: a short one corresponding to the double bond, and a long one corresponding to the single bond in the dominant product VB structure (cf. $\mathbf{3}_{P1}$ in Figure 5).

Let us consider now how this loss of resonance energy impacts the PES exactly by constructing the VBSCD associated with the reaction under consideration (Figure 6).

In the reactant geometry, the reactant state R is resonance stabilized due to the interaction between the localized $\mathbf{1}_R$ and $\mathbf{2}_R$ states; *vide supra* (Figure 4a). The excited reactant state (R*) can be expected to be equally delocalized in this geometry: $\mathbf{3}_{P1}$ and $\mathbf{4}_{P2}$ are degenerate in the reactant geometry, and hence they will contribute equally to the wave function. On the product side, the product state P is—as mentioned—localized. Since P* corresponds to the vertical excitation of P, this state shares the same (localized) geometry of the product, and hence, it will also be mainly localized (though it can retain a partial delocalized character in the case that the geometrical differences between R and P are not too significant, *vide infra*).

As such, for a delocalized species undergoing a (localization) reaction, the product states are both destabilized relative to the reactant states in the VBSCD. The extent of destabilization is related to the resonance energy present in the reactant state but usually does not correspond quantitatively to this quantity: the previously mentioned geometric relaxation of the system throughout the reaction increasingly accommodates—and thus stabilizes—the emerging dominant product VB structure, which compensates part of the resonance energy loss. For our model H-abstraction reaction involving the delocalized allyl radical, we obtain a thermodynamic driving force ΔE_{rp} of +5.7 kcal/mol. Thus, since ΔE_{rp} for the corresponding reaction involving the localized $H_3C^\bullet$ amounted to −13.4 kcal/mol (cf. the previous section), one can estimate the actual relative destabilization of the product state for this specific localized product at 19.1 kcal/mol. Hence, the total amount of resonance energy present in the reactant state should be considered as an upper limit and a guide value for the relative product destabilization.

According to the Bell−Evans−Polanyi principle,[28] a destabilization of the product compared to the reactant, i.e., a decrease in the thermodynamic driving force ΔE_{rp}, should induce an increase in the activation energy associated with the reaction. A similar expectation emerges from analysis of the approximate reaction barrier height equation introduced in the previous section, cf. eq 2: given that $\Delta\Delta E_{rp}$ amounted to 19.1 kcal/mol when comparing the H-abstraction reaction involving $H_3C^\bullet$ with the one involving allyl$^\bullet$, one can estimate $\Delta\Delta E^{\ddagger}$ to amount to approximately 9.5 kcal/mol, assuming that the other factors in the expression remain more or less constant. This is exactly what emerges from our UB3LYP/cc-pVTZ calculations: $\Delta E^{\ddagger}$ amounts to 6.9 kcal/mol for $H_3C^\bullet$, and for allyl$^\bullet$ $\Delta E^{\ddagger}$ is calculated to amount to 16.5 kcal/mol (Figure 7).

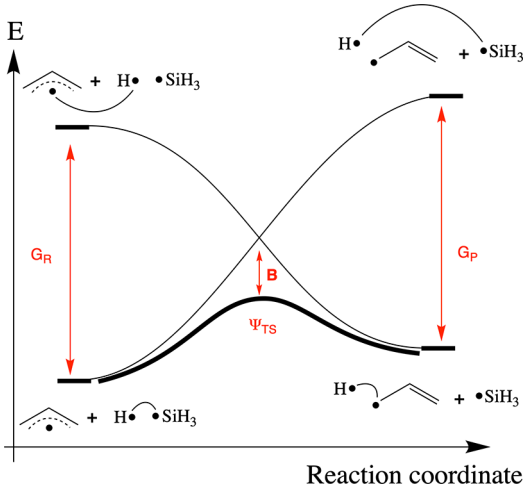

Figure 6. VB reactivity diagram for the H-abstraction reaction between allyl$^\bullet$ and H−SiH_3.

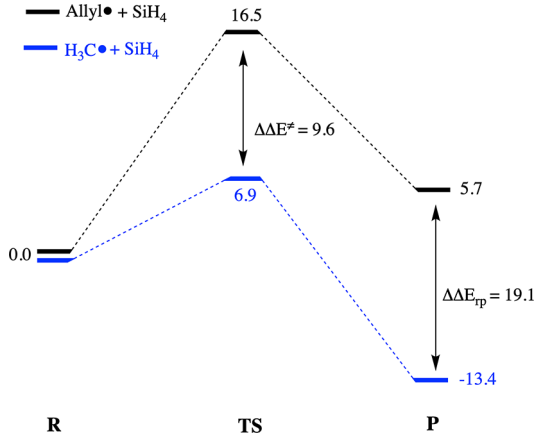

Figure 7. Potential energy surface for the hydrogen abstraction reaction of allyl$^\bullet$ and $H_3C^\bullet$ with SiH_4. Calculations were performed at the UB3LYP/cc-pVTZ level of theory. Energies are denoted in kcal/mol (ZPE included).

https://dx.doi.org/10.1021/jacs.0c02390
J. Am. Chem. Soc. 2020, 142, 10102−10113

So far, we have only focused on a single prototypical radical reaction type, i.e., H-abstraction. However, it is important to underscore that our analysis is universally valid: consider, for example, the PESs associated with the radical addition reaction involving respectively $H_3C^\bullet$ and allyl$^\bullet$ with ethylene (Figure 8). Now, our calculations indicate that $\Delta\Delta E_{rp}$ amounts to 17.4 kcal/mol, and this relative product destabilization gives rise to a $\Delta E^{\ddagger}$ of 7.3 kcal/mol.

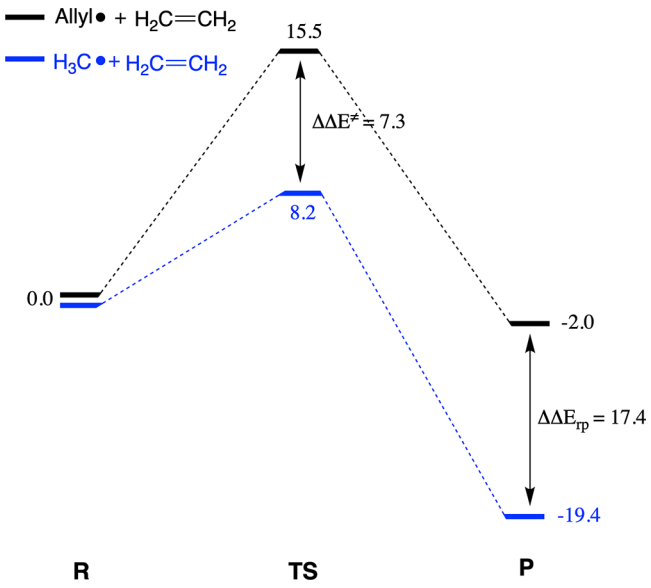

Figure 8. Potential energy surface for the addition reaction of allyl$^\bullet$ and $H_3C^\bullet$ with ethylene. Calculations were performed at the UB3LYP/cc-pVTZ level of theory. Energies are denoted in kcal/mol (ZPE included).

Spin Density Distribution as a Probe for the Regioselective Preference. In the previous two sections, we have explored how spin delocalization affects the PES associated with a radical reaction by considering a prototypical localized and delocalized radical: delocalization energy acts in the first place as a thermodynamic penalty, destabilizing localized products relative to their corresponding delocalized reactants. This relative product destabilization not only causes a decrease in the thermodynamic driving force (ΔE_{rp}) but also induces a commensurate increase in the reaction barrier height ($\Delta E^{\ddagger}$)[17,18] according to the Bell−Evans−Polanyi principle. Additionally, we have already briefly discussed how the extent of delocalization within a molecule can be gauged through inspection of the local spin density distribution: localized radicals have a single radical center for which the spin density approaches unity; for delocalized radicals, the spin density is spread out over several centers. As mentioned in the Introduction, the literature is abound with data corroborating the conclusions of this analysis and underscoring its universal validity for organic (C-based) compounds: the role of the spin density distribution as a local reactivity indicator to infer reactivity trends in radicals and (di/poly)radicals alike has been accepted for quite some time already.[6]

In the present section, we will illustrate how, starting from this knowledge, the spin density distribution emerges as a natural reactivity indicator for radical molecules containing multiple reactive sites, able to infer the "most favorable" reaction pathway, i.e., the regioselectivity. Once more, we will focus on an example compound, the enol radical (H_2C=CHO$^\bullet$) shown in Figure 9a. A simple electronic structure calculation reveals that the radical electron in this compound is

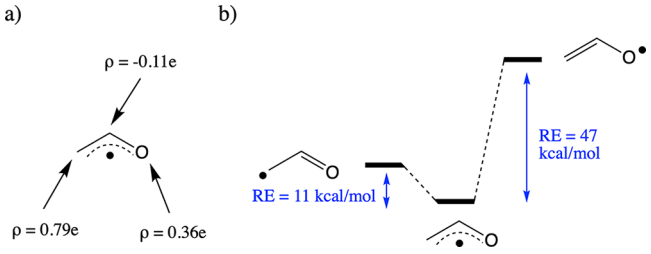

Figure 9. (a) NBO spin density distribution for the vinyloxy radical, calculated at the UB3LYP/cc-pVTZ level of theory. (b) Interaction between the localized resonance structure giving rise to the delocalized ground state of vinyloxy$^\bullet$ (H_2C=CHO$^\bullet$). Resonance energies were calculated at the VBSCF/6-311++G** level of theory.

mainly localized on the outermost C-center: the NBO spin density on this atom amounts to 0.79e, the O-atom on the other end of the molecule carries a spin density of 0.36e, and the middle C-atom carries −0.11e.

In agreement with these calculated spin densities, we find that the localized VB structure in which the unpaired electron resides on the C-atom is significantly more stable than the one in which the radical resides on the O-atom: for the former structure, the resonance energy separating it from the delocalized resonance hybrid amounts to only 11 kcal/mol, whereas for the latter, this resonance energy amounts to almost 47 kcal/mol (Figure 9b). As such, given the analysis in the previous section, one can reasonably expect that this radical compound will preferentially engage in radical reactivity through the C-center: reacting from this side of the molecule causes a much smaller loss of delocalization energy throughout the reaction.

In Figure 10, we show the calculated PESs for both reaction pathways, together with their respective localized analogues, i.e., the H-abstraction from SiH_4 by $H_3C^\bullet$ and HO$^\bullet$. It should be noted that, for the considered pathways of the vinyloxy radical, the change in $\Delta E^{\ddagger}$ compared to the respective localized analogue estimated from eq 2 is not quantitatively identical to half the amount of resonance energy lost throughout the reaction, i.e., $\Delta\Delta E_{rp}$ (cf. eq 3). The reason for these apparent deviations is obviously connected to non-negligible shifts in the other factors in this equation, i.e., changes to the curvature (the f_0-factor), the promotion energies on the reactant and product side (G_R and G_P), and the resonance energy in the TS geometry (B).[15,16] Nevertheless, the trends outlined in the previous section are clearly preserved: the less the radical electron is localized on a specific site (as probed by the spin density distribution), the higher the amount of delocalization energy lost throughout the reaction involving this site, which is reflected in a rise of ΔE_{rp} compared to the localized reaction analogue, as well as a commensurate increase of $\Delta E^{\ddagger}$.

It should be clear from Figure 10 that inspection of the spin density distribution leads to the correct regioselectivity for the vinyloxy radical: the H-abstraction reaction will preferentially take place from the site with the highest spin density, i.e., the C-side. As such, the spin density is indeed a very useful local reactivity descriptor to estimate the preferential reaction pathway, i.e., the regioselectivity, for this molecule.

It should be noted that—as an added bonus—our foregoing analysis straightforwardly reveals the general condition which

https://dx.doi.org/10.1021/jacs.0c02390
J. Am. Chem. Soc. 2020, 142, 10102−10113

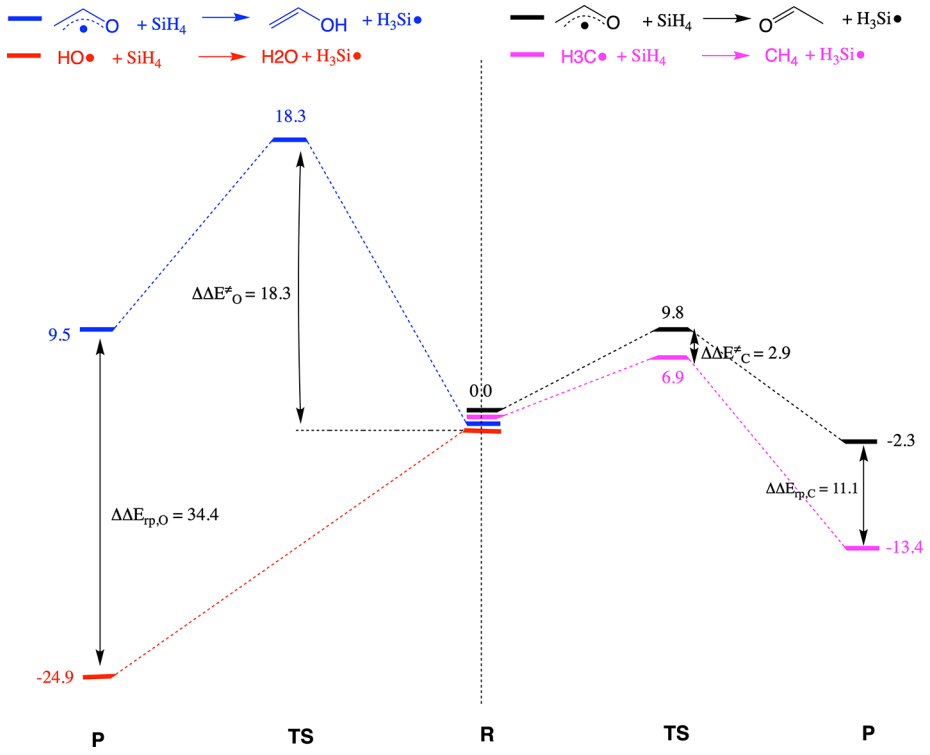

Figure 10. Potential energy surfaces for the H-abstraction reactions from SiH_4 involving the O-moiety (left-hand side; the blue profile) and C-moiety (right-hand side; the black profile) of vinyloxy$^\bullet$, together with their corresponding localized analogues $HO^\bullet$ and $H_3C^\bullet$ (red and lilac profiles, respectively). Energies are denoted in kcal/mol (ZPE included). Note that the reaction between $HO^\bullet$ and SiH_4 (red profile) is essentially barrierless at the level of theory considered (UB3LYP/cc-pVTZ); the thermodynamic driving force is so significant that the reactants spontaneously react upon encounter.

leads to correct prediction of radical reactivity trends and regioselectivity from spin densities: the difference in delocalization penalty for the two sites of the delocalized molecule has to exceed the difference in thermodynamic driving forces between the corresponding localized species $\Delta\Delta E_{\text{rp-local}}$, i.e., $\Delta E_{\text{rp,HO}^\bullet} - \Delta E_{\text{rp,H}_3\text{C}^\bullet}$. In Figure 10, $\Delta\Delta E_{\text{rp-local}}$ for the localized analogues ($HO^\bullet$ and $H_3C^\bullet$) amounted to −11.5 kcal/mol, i.e., −24.9 − (−13.4) kcal/mol, and the difference in delocalization penalty amounted to 23.3 kcal/mol, i.e., 34.4 − 11.1 kcal/mol. It is only because the magnitude of the latter value exceeds the former that the site of the delocalized molecule exhibiting the highest spin density (the C-atom) corresponds to the most thermodynamically stable product. If the difference in delocalization energy would have been lower than $\Delta\Delta E_{\text{rp-local}}$, then the inherent reactivity difference of $HO^\bullet$ compared to $H_3C^\bullet$ would have overridden the delocalization effect, so that an attack at the O-site, which carries the lowest spin density, would have corresponded to a slightly higher thermodynamic driving force than an attack at the C-site.

For organic molecules in general, this spin density-based strategy can be expected to work reasonably well, since the delocalized systems typically exhibit a very limited diversity in their elemental composition, and the magnitude of the delocalization in these compounds is usually significant compared to the differences in inherent reactivity among the localized analogues. Plenty of experimental and theoretical evidence exists to circumstantiate this assertion.[6]

Potential Pitfalls and Exceptions: The Extraordinary Case of O_2. The previous sections may have given the impression that analysis of spin density distributions is an almost foolproof approach to probe the relative magnitude of the delocalization energy loss associated with a delocalized species upon reaction, and—as a consequence—to infer reactivity trends among series of (di/poly)radical compounds and regioselectivities. In the present section, we want to stress that this is not always the case, since spin density distributions do not always reveal the full intricate complexity of the wave function associated with the compound under consideration.

The best example to illustrate the limitations of the spin density approach is the extraordinary O_2 molecule. The triplet state of this diatomic molecule contains two unpaired electrons, and hence, the spin density on either of the two O-atoms making up this molecule amounts to 1e. Based on our previous analysis, this seemingly localized nature of the radical electrons in O_2 could lead to the false impression that this molecule should undergo reaction in a similar fashion as the $HO^\bullet$ radical: the H-abstraction from SiH_4, for example, should be an (almost) barrierless and highly exothermic process due to the seemingly localized radical electrons. Fortunately, every reader can attest that this is most definitely not what happens in reality: we obviously do not combust spontaneously upon exposure to the earthly atmosphere full of $^3O_2$ surrounding us![29]

The root cause for this apparent contradiction can be found in the extraordinary electronic structure of this species: in contrast to what one would conclude from a naive analysis of the spin density distribution, this molecule is, in reality, highly resonance stabilized. A simple molecular orbital diagram for O_2 reveals that the frontier orbitals of this compound consist of two pairs of degenerate orbitals—respectively π_x,π_y and π_x^*,π_y^*—emerging from the individual p_x and p_y atomic

https://dx.doi.org/10.1021/jacs.0c02390
J. Am. Chem. Soc. 2020, 142, 10102−10113

orbitals. Four different VB structures arise from the distribution of six electrons—four of α-spin and two of β-spin—over these four valence $2p_x$-π and $2p_y$-π atomic orbitals in the triplet ground state of this compound (Figure 11).

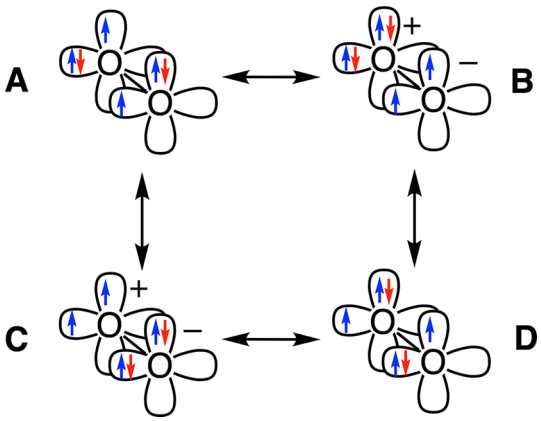

Figure 11. Four main VB structures **A**−**D**, contributing to the ground state of $^3O_2$. The four α-spin electrons each occupy one of the four 2p-π atomic orbitals, so that only the β-spin electrons (in red) are delocalized.

The four VB structures depicted in Figure 11 interact significantly; calculations at the VBSCF/6-311++G** level of theory performed within the context of the present study indicate that the total resonance energy, i.e., the energy difference between one of the isolated lowest-energy structures (**A** and **D**) and the full resonance hybrid, amounts to 79 kcal/mol.[30] The presence of this resonance energy will obviously impact the PESs associated with any reaction involving this delocalized species. One can straightforwardly estimate the "resonance penalty" associated with reactions involving this molecule by realizing that structures **A** and **D** individually correspond to fully localized (double) radicals; i.e., they are more or less equivalent to the fully localized HO$^\bullet$. Hence, the resonance penalty relative to HO$^\bullet$ should not be far off from the total resonance energy present in the π-system, i.e., 79 kcal/mol. Indeed, our calculations reveal that the H-abstraction reaction from SiH_4 by delocalized $^3O_2$ is 64 kcal/mol more endothermic than the corresponding reaction by HO$^\bullet$ (Table 1). In analogy to what we observed before, this

Table 1. Comparison of the Barrier Heights ($\Delta E^{\ddagger}$) and Reaction Energies (ΔE_{rp}) of H-Abstraction from SiH_4 and Addition to Ethylene for $^3O_2$ and HO$^\bullet$

	H-abstraction from SiH_4		addition to ethylene	
	$\Delta E^{\ddagger}$ (kcal/mol)	ΔE_{rp} (kcal/mol)	$\Delta E^{\ddagger}$ (kcal/mol)	ΔE_{rp} (kcal/mol)
$^3O_2$	39.2	39.2	32.9	32.7
HO$^\bullet$	–	−24.9	–	−24.7

difference in ΔE_{rp} is translated into an increase in $\Delta E^{\ddagger}$ by 39 kcal/mol. Similar results are also found for the addition reactions to ethylene.

We would like to end this section by emphasizing that the relative inertness of $^3O_2$ should not be considered as a violation or repudiation of the VB delocalization perspective. Rather, it is a prime example of a situation where the spin density distribution does not capture the inherent delocalization, in two perpendicular planes (cf. Figure 11), present within the wave function.

Extending the VB Delocalization Perspective to Other Local Reactivity Descriptors: The Case of the Fukui Function. So far, the only local reactivity descriptor we have considered was the spin density distribution. The goal of the present section is to demonstrate that our approach can straightforwardly be extended to other reactivity descriptors as well. We will focus specifically on the Fukui function, a local reactivity descriptor associated with nucleophilic/electrophilic reactivity which emerges from conceptual DFT.[31] Once more, let us turn to a model reaction: the methylation of (the ambident) vinyloxy anion (cf. Figure 12).

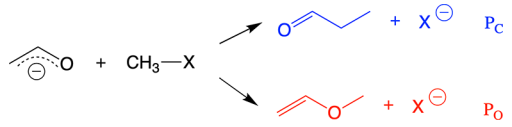

Figure 12. Possible outcomes for the methylation reaction between vinyloxy anion and CH_3X (X = Cl, I, Br, ...).

Analogously to the case of the vinyloxy radical discussed before, vinyloxy anion can react in two different ways: either through the C-site or through the O-site. Within a conceptual DFT approach, the most nucleophilic site of this compound is usually probed by the spatial distribution of the Fukui function for electrophilic attack $f^-(r)$,[1−3,32]

$$f^-(\boldsymbol{r}) = \left(\partial\rho(\boldsymbol{r})/\partial N\right)^- = \rho_N(\boldsymbol{r}) - \rho_{N-1}(\boldsymbol{r}) \approx |\Psi^2_{\mathrm{HOMO}}| \quad (4)$$

where $\rho(\boldsymbol{r})$ corresponds to the electron density and N corresponds to the number of electrons in the compound.

Let us now show how the Fukui function emerges within our qualitative VB framework by constructing the VBSCD associated with this reaction. For nucleo-/electrophilic reactions, the product-state curve, i.e., the curve connecting the promoted reactant state (R*) to the product state (P) in the VBSCD (*vide supra*), corresponds to an excited charge-transfer state. In the case of the reaction considered here, the relevant CT state is the one in which an electron is transferred from the vinyloxy anion to H_3C−X, as shown in Figure 13a. As such, R* corresponds to an isolated vinyloxy radical and an equally isolated σ*-radical anion H_3C−X$^-$. The vinyloxy radical species in R* will obviously be delocalized: it is a hybrid of one localized structure in which the unpaired electron resides on the C-atom and one in which this radical electron resides on the O-atom (*vide supra*; cf. Figure 9b).

As the reaction proceeds, i.e., as one advances from R toward P, the resonance energy between these two localized structures in this vinyloxy radical in the product state curve will be lost: the methylation occurs on either the C- or O-side. As such, one can expect that the most stable product will be associated with the localized VB structure with the highest weight in the promoted product state R*, since the corresponding mode of attack will involve the lowest "resonance penalty" to be paid. Hence, based on Figure 9b, one can infer that the C-attack will be the most thermodynamically favorable reaction pathway. Figure 13b enables one to visualize the specific product state curves associated with the two competing reaction pathways.

https://dx.doi.org/10.1021/jacs.0c02390
J. Am. Chem. Soc. 2020, 142, 10102−10113

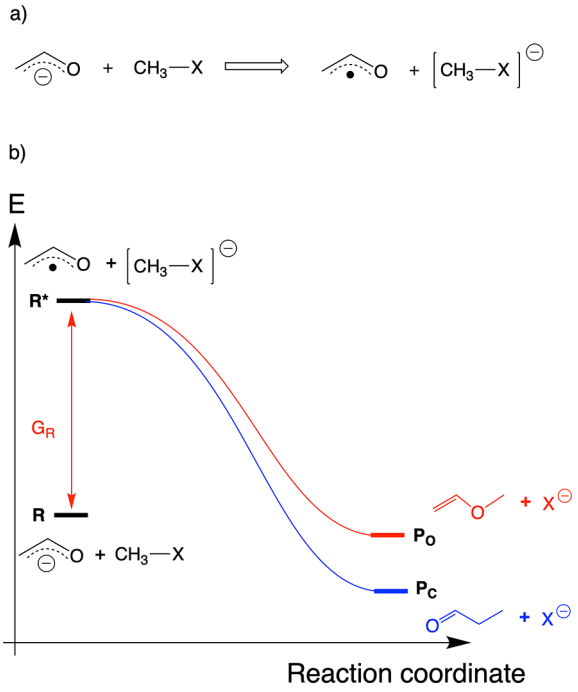

Figure 13. (a) The CT state in the reactant geometry corresponding to the product state curve in the VBSCD for the methylation reaction of vinyloxy anion. (b) The specific product state curves associated with the two competing reaction pathways.

Previous calculations performed by Mayr and co-workers confirm the analysis so far: even though the absolute ΔE_{rp} values coming out of their calculations were determined to be highly dependent on the nature of the halogen in H_3C-X, the relative difference in thermodynamic driving force between the C- and O-attack, i.e., $\Delta\Delta E_{rp}$, consistently amounted to approximately 20 kcal/mol in favor of the C-attack.[12]

Let us now take a moment to contemplate what we have achieved so far. We have demonstrated that, for nucleophilic attack involving an ambident reactant, the thermodynamic stability of the individual products is determined by the corresponding "resonance/delocalization penalty", in a similar way as it was demonstrated to be the case for (di)radical reactions. Contrary to our analysis in the previous sections, the resonance penalty cannot be probed now simply by considering spin density distributions. Instead, one ought to analyze *the delocalization of the radical electron which emerges in the ambident reactant after one electron has been removed from this species*. Effectively, this delocalization can be probed by considering the distribution of the highest occupied molecular orbital of the nucleophile, i.e., the HOMO, since from an MO perspective, the radical electron emerging from the removal of an electron from the species will be located in this orbital. Turning back now to eq 4 at the beginning of this section, one should realize that *we have effectively recovered the idea of a Fukui function as a local reactivity descriptor from a purely VB perspective!* Indeed, one finds that the HOMO of vinyloxy anion is disproportionally localized on the extremal C-atom (Figure 14), and consequently, the atom-condensed Fukui function in vinyloxy anion has a much higher amplitude on this site as well (ρ(C) = 0.53e, ρ(O) = 0.34e; cf. Computational Details).

Let us now complete the construction of the VBSCD which we started in Figure 13. What is still missing in this diagram are

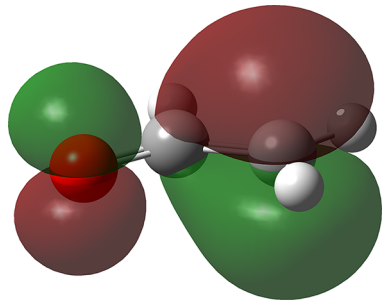

Figure 14. HOMO orbital of vinyloxy anion calculated at the B3LYP/cc-pVTZ level of theory. Note that the orbital is mainly located on the extremal C-atom.

the reactant state curves. Obviously, the shape and curvature of these state curves will be governed by the relative stability of their respective end points, i.e., the excited product state P*. Which product geometry will stabilize the electronic structure of the reactant state the most? This can be straightforwardly inferred by considering the VB composition of the delocalized vinyloxy anion species (Figure 15).

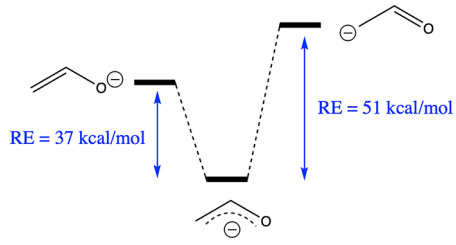

Figure 15. Interaction between the localized resonance structure giving rise to the delocalized ground state of vinyloxy anion. Resonance energies were calculated at the VBSCF/6-311++G** level of theory.

From Figure 15, one can clearly conclude that this species is best described by the localized VB structure in which the negative charge resides on the oxygen moiety. One can logically expect that a product geometry stabilizing this dominant localized VB structure will be lower in energy than one in which this dominant structure is destabilized. As such, the excited product P* associated with the O-attack reaction pathway ought to be more stable than the one associated with the C-attack pathway for the reaction under consideration. Completing the diagram in Figure 13 this way, one ends up with the VBSCD shown in Figure 16.

Note that according to Figure 16, $G_{P,O} < G_{P,C}$. Hence, we now have two counteracting factors influencing the barrier heights of the respective reaction pathways, cf. eq 3. Whereas the thermodynamic driving force relatively stabilizes the reaction barrier associated with the C-pathway, the promotion energy (on the product side) relatively stabilizes the reaction barrier associated with the O-side.

Which one of these two reaction pathways would be kinetically favored; i.e., which one of these pathways exhibits the lowest barrier in reality? Obviously, this depends on which one of the two factors impacting the activation energies dominates; the previously mentioned calculations performed by Mayr et al. indicate that, for the specific reaction considered here, the O-methylation reaction pathway exhibits a slightly lower activation energy than the C-pathway ($\Delta\Delta E^{\ddagger}$ = 2−3

https://dx.doi.org/10.1021/jacs.0c02390
J. Am. Chem. Soc. 2020, 142, 10102−10113

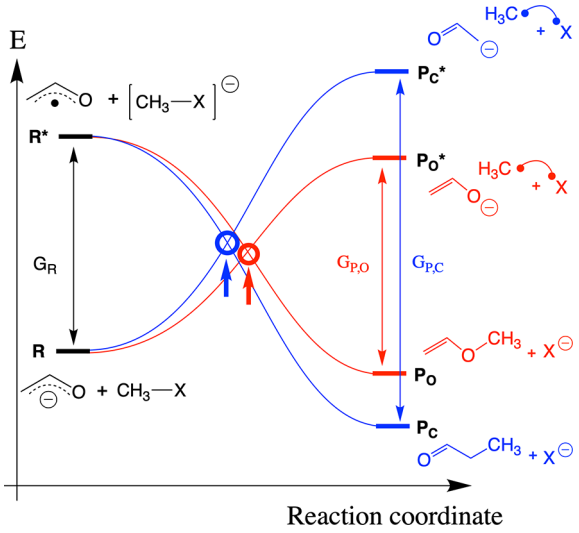

Figure 16. Completed VBSCD for the methylation reaction of vinyloxy anion. Note that, due to the difference in $G_{P,O}$ and $G_{P,C}$, the crossing point between the reactant and product curves for the O-attack is not necessarily higher in energy than that for the C-attack, so that the former pathway can become kinetically favored, even though the latter pathway exhibits the highest thermodynamic driving force, as indicated before.

kcal/mol).[12] Plenty of other ambident nucleophiles and electrophiles are known to exhibit a similar behavior; i.e., the exhibited kinetic preference differs from the thermodynamic preference.[11,13]

Note that the observation that kinetic and thermodynamic preferences do not generally agree in electrophilic/nucleophilic reactions is in contrast with the radical reactivity analyzed in the previous sections. There, one could safely assume that, in most cases, the differences in ΔE_{rp} would dominate the reaction barrier heights $\Delta E^{\ddagger}$. Due to the charge-transfer relationship between the two state curves making up the VBSCD for nucleophilic/electrophilic reactions, this is not the case here anymore.

Hence, even though the Fukui function, i.e., the spatial HOMO/LUMO distributions, can be extremely useful to infer general reactivity trends for electrophilic/nucleophilic reactivity, its accuracy in predicting the product selectivity in ambident reactivity is limited. This local reactivity descriptor will generally point to the thermodynamically favored reaction pathway, but the kinetics—which govern the product selectivities in most cases—do not always follow suit.

CONCLUSIONS

In the present contribution, we have examined how local reactivity descriptors shape the potential energy surface associated with chemical reactions. We demonstrated that many common local descriptors, e.g., the spin density distribution for radical reactions and the Fukui function for electro-/nucleophilic reactions, can essentially be regarded—in one way or another—as indirect measures of delocalization, i.e., resonance stabilization, of the reactants within (qualitative) VB theory. The inherent connection between (spatial) delocalization and (energetic) resonance stabilization embedded in this theory provides a natural and elegant framework through which the impact of individual local reactivity descriptors on the global PES can be analyzed and understood.

Through consideration of a set of simple—yet relevant—model systems, we laid out some general conditions under which these descriptors can be expected to succeed at predicting reactivity trends and regioselectivities, and when they can be expected to go astray.

For (di)radical reactions, we demonstrated that the delocalization/resonance penalty associated with specific reaction pathways will affect in the first place the thermodynamic driving force, ΔE_{rp}, which in its turn induces a modification of the corresponding activation energy, $\Delta E^{\ddagger}$, according to the Bell−Evans−Polanyi principle. As such, as long as the differences in resonance penalty between two pathways exceed the inherent difference in ΔE_{rp} between the respective localized analogues, one can infer both thermodynamic and kinetic preference from analysis of the spin density distributions.

For nucleophilic/electrophilic reactions, the Fukui function plays a similar role as the spin density distribution for radical reactions in shaping the state curves in the VBSCD associated with the reaction, but with the important distinction that it is now only the product state curve which is affected by this descriptor. Hence, analysis of the Fukui function will generally lead to the identification of the thermodynamically favored product, but the kinetic preference is not necessarily the thermodynamically preferred one. This offers a clear explanation for the failure of Fukui function analysis to correctly predict the experimentally observed (kinetic) product selectivities for ambident reactivity.

Overall, our analysis provides new insights into the role played by—as well as the limitations of—local reactivity descriptors. The present contribution effectively *forms a first bridge between two seemingly detached and irreconcilable realms within chemical theory: conceptual density functional theory and valence bond theory*. We anticipate that further interplay between these two theories will lead to a productive synergy which may induce enhanced conceptual understanding of various chemical problems.[20]

ASSOCIATED CONTENT

Supporting Information

The Supporting Information is available free of charge at https://pubs.acs.org/doi/10.1021/jacs.0c02390.

Weights of the individual VB structures, barrier heights and reaction energies computed at UB3LYP/6-311++G** level of theory, geometries and electronic energies for all the calculated systems (PDF)

AUTHOR INFORMATION

Corresponding Authors

Thijs Stuyver − *Institute of Chemistry, The Hebrew University, Jerusalem 91904, Israel; Algemene Chemie, Vrije Universiteit Brussel, 1050 Brussels, Belgium;* orcid.org/0000-0002-8322-0572; Email: thijs.stuyver@mail.huji.ac.il

Sason Shaik − *Institute of Chemistry, The Hebrew University, Jerusalem 91904, Israel;* orcid.org/0000-0001-7643-9421; Email: sason.shaik@gmail.com

Authors

Frank De Proft − *Algemene Chemie, Vrije Universiteit Brussel, 1050 Brussels, Belgium;* orcid.org/0000-0003-4900-7513

Paul Geerlings − *Algemene Chemie, Vrije Universiteit Brussel, 1050 Brussels, Belgium;* orcid.org/0000-0003-1897-7285

https://dx.doi.org/10.1021/jacs.0c02390
J. Am. Chem. Soc. 2020, 142, 10102−10113

Complete contact information is available at:
https://pubs.acs.org/10.1021/jacs.0c02390

Notes

The authors declare no competing financial interest.

■ ACKNOWLEDGMENTS

T.S. acknowledges the Research Foundation-Flanders (FWO) for a position as postdoctoral research fellow (1203419N). F.D. and P.G. acknowledge the Vrije Universiteit Brussel (VUB) and the Research Foundation Flanders (FWO) for continuous support to the ALGC research group. Among others, the Strategic Research Program funding of the VUB is thanked for financial support. S.S. is supported by the Israel Science Foundation (ISF 520/18).

■ REFERENCES

(1) Yang, W.; Parr, R. G. *Density Functional Theory of Atoms and Molecules*; Oxford University Press: Oxford, 1989.
(2) Geerlings, P.; De Proft, F.; Langenaeker, W. Conceptual density functional theory. *Chem. Rev.* **2003**, *103*, 1793−1874.
(3) For a recent status report, see: Geerlings, P.; Chamorro, E.; Chattaraj, P. K.; De Proft, F.; Gázquez, J. L.; Liu, S.; Morell, C.; Toro-Labbé, A.; Vela, A.; Ayers, P. Conceptual density functional theory: status, prospects, issues. *Theor. Chem. Acc.* **2020**, *139*, 36.
(4) Parr, R. G.; Yang, W. Density functional approach to the frontier-electron theory of chemical reactivity. *J. Am. Chem. Soc.* **1984**, *106*, 4049−4050.
(5) Yang, W.; Parr, R. G. Hardness, softness, and the fukui function in the electronic theory of metals and catalysis. *Proc. Natl. Acad. Sci. U. S. A.* **1985**, *82*, 6723−6726.
(6) Stuyver, T.; Chen, B.; Zeng, T.; Geerlings, P.; De Proft, F.; Hoffmann, R. Do Diradicals Behave Like Radicals? *Chem. Rev.* **2019**, *119*, 11291−11351.
(7) Damoun, S.; Van de Woude, G.; Mendez, F.; Geerlings, P. Local softness as a regioselectivity indicator in [4+ 2] cycloaddition reactions. *J. Phys. Chem. A* **1997**, *101*, 886−893.
(8) Aurell, M. J.; Domingo, L. R.; Pérez, P.; Contreras, R. A theoretical study on the regioselectivity of 1, 3-dipolar cycloadditions using DFT-based reactivity indexes. *Tetrahedron* **2004**, *60*, 11503−11509.
(9) Melin, J.; Aparicio, F.; Subramanian, V.; Galvan, M.; Chattaraj, P. K. Is the Fukui Function a Right Descriptor of Hard- Hard Interactions? *J. Phys. Chem. A* **2004**, *108*, 2487−2491.
(10) Jaque, P.; Toro-Labbé, A.; Geerlings, P.; De Proft, F. Theoretical study of the regioselectivity of [2 + 2] photocycloaddition reactions of acrolein with olefins. *J. Phys. Chem. A* **2009**, *113*, 332−344.
(11) Mayr, H.; Breugst, M.; Ofial, A. R. Farewell to the HSAB treatment of ambident reactivity. *Angew. Chem., Int. Ed.* **2011**, *50*, 6470−6505.
(12) Breugst, M.; Zipse, H.; Guthrie, J. P.; Mayr, H. Marcus analysis of ambident reactivity. *Angew. Chem., Int. Ed.* **2010**, *49*, 5165−5169.
(13) Bettens, T.; Alonso, M.; De Proft, F.; Hamlin, T. A.; Bickelhaupt, F. M. Ambident Nucleophilic Substitution: Understanding Non-HSAB Behavior through Activation Strain and Conceptual DFT Analyses. *Chem. - Eur. J.* **2020**, *26*, 3884−3893.
(14) (a) Hoffmann, R.; Woodward, R. B. Conservation of orbital symmetry. *Acc. Chem. Res.* **1968**, *1*, 17−22. (b) Fukui, K.; Yonezawa, T.; Shingu, H. A molecular orbital theory of reactivity in aromatic hydrocarbons. *J. Chem. Phys.* **1952**, *20*, 722−725.
(15) Shaik, S. S.; Hiberty, P. C. *A chemist's guide to valence bond theory*; John Wiley & Sons, 2007.
(16) Shaik, S.; Shurki, A. Valence bond diagrams and chemical reactivity. *Angew. Chem., Int. Ed.* **1999**, *38*, 586−625.
(17) Lai, W.; Li, C.; Chen, H.; Shaik, S. Hydrogen-abstraction reactivity patterns from A to Y: the valence bond way. *Angew. Chem., Int. Ed.* **2012**, *51*, 5556−5578.
(18) Usharani, D.; Lai, W.; Li, C.; Chen, H.; Danovich, D.; Shaik, S. A tutorial for understanding chemical reactivity through the valence bond approach. *Chem. Soc. Rev.* **2014**, *43*, 4968−4988.
(19) Shaik, S. What happens to molecules as they react? A valence bond approach to reactivity. *J. Am. Chem. Soc.* **1981**, *103*, 3692−3701.
(20) Hiberty, P. C.; Braïda, B. Pleading for a Dual Molecular-Orbital/Valence-Bond Culture. *Angew. Chem., Int. Ed.* **2018**, *57*, 5994−6002.
(21) (a) Becke, A. D. Density-functional exchange-energy approximation with correct asymptotic behavior. *Phys. Rev. A: At., Mol., Opt. Phys.* **1988**, *38*, 3098−3100. (b) Lee, C.; Yang, W.; Parr, R. G. Development of the Colle-Salvetti correlation-energy formula into a functional of the electron density. *Phys. Rev. B: Condens. Matter Mater. Phys.* **1988**, *37*, 785−789. (c) Stephens, P. J.; Devlin, F. J.; Chabalowski, C.; Frisch, M. J. Ab initio calculation of vibrational absorption and circular dichroism spectra using density functional force fields. *J. Phys. Chem.* **1994**, *98*, 11623−11627.
(22) Frish, M. J.; Trucks, G. W.; Schlegel, H. B.; Scuseria, G. E.; Robb, M. A.; Cheeseman, J. R.; Scalmani, G.; Barone, V.; Mennucci, B.; Petersson, G. A.; Nakatsuji, H.; Caricato, M.; Li, X.; Hratchian, H. P.; Izmaylov, A. F.; Bloino, J.; Zheng, G.; Sonnenberg, J. L.; Hada, M.; Ehara, M.; Toyota, K.; Fukuda, R.; Hasegawa, J.; Ishida, M.; Nakajima, T.; Honda, Y.; Kitao, O.; Nakai, H.; Vreven, T.; Montgomery, J. A., Jr.; Peralta, J. E.; Ogliaro, F.; Bearpark, M.; Heyd, J. J.; Brothers, E.; Kudin, K. N.; Staroverov, V. N.; Keith, T.; Kobayashi, R.; Normand, J.; Raghavachari, K.; Rendell, A.; Burant, J. C.; Iyengar, S. S.; Tomasi, J.; Cossi, M.; Rega, N.; Millam, J. M.; Klene, M.; Knox, J. E.; Cross, J. B.; Bakken, V.; Adamo, C.; Jaramillo, J.; Gomperts, R.; Stratmann, R. E.; Yazyev, O.; Austin, A. J.; Cammi, R.; Pomelli, C.; Ochterski, J. W.; Martin, R. L.; Morokuma, K.; Zakrzewski, V. G.; Voth, G. A.; Salvador, P.; Dannenberg, J. J.; Dapprich, S.; Daniels, A. D.; Farkas, O.; Foresman, J. B.; Ortiz, J. V.; Cioslowski, J.; Fox, D. J. *Gaussian 09*, revision D.01; Gaussian, Inc.: Wallingford, CT, 2013.
(23) Reed, A. E.; Weinstock, R. B.; Weinhold, F. Natural population analysis. *J. Chem. Phys.* **1985**, *83*, 735−746.
(24) (a) Song, L.; Mo, Y.; Zhang, Q.; Wu, W. XMVB: a program for ab initio nonorthogonal valence bond computations. *J. Comput. Chem.* **2005**, *26*, 514−521. (b) Chen, Z.; Ying, F.; Chen, X.; Song, J.; Su, P.; Song, L.; Mo, Y.; Zhang, Q.; Wu, W. XMVB 2.0: A new version of Xiamen valence bond program. *Int. J. Quantum Chem.* **2015**, *115*, 731−737.
(25) (a) Gu, J.; Wu, W.; Danovich, D.; Hoffmann, R.; Tsuji, Y.; Shaik, S. Valence bond theory reveals hidden delocalized diradical character of polyenes. *J. Am. Chem. Soc.* **2017**, *139*, 9302−9316. (b) Gu, J.; Wu, W.; Stuyver, T.; Danovich, D.; Hoffmann, R.; Tsuji, Y.; Shaik, S. Cross Conjugation in Polyenes and Related Hydrocarbons: What Can Be Learned from Valence Bond Theory about Single-Molecule Conductance? *J. Am. Chem. Soc.* **2019**, *141*, 6030−6047.
(26) Shaik, S.; Hiberty, P. C. Valence bond, its history, fundamentals and applications: A primer. *Rev. Comput. Chem.* **2004**, *20*, 1.
(27) These parameters are generally valid for reactions without significant steric hindrance, i.e., all the radical reactions considered in this manuscript. In the case that steric hindrance is significant, the f_0 parameter can be expected to be larger, corresponding to a relative elevation of the crossing point of the diabatic reactant and product curve.
(28) (a) Bell, R. P. The theory of reactions involving proton transfers. *Proc. R. Soc. A* **1936**, *154*, 414−429. (b) Evans, M. G.; Polanyi, M. Further considerations on the thermodynamics of chemical equilibria and reaction rates. *Trans. Faraday Soc.* **1936**, *32*, 1333−1360.
(29) (a) Borden, W. T.; Hoffmann, R.; Stuyver, T.; Chen, B. Dioxygen: what makes this triplet diradical kinetically persistent? *J. Am. Chem. Soc.* **2017**, *139*, 9010−9018. See also: (b) Filatov, M.;

Reckien, W.; Peyerimhoff, S. D.; Shaik, S. What are the reasons for the kinetic stability of a mixture of H_2 and O_2? *J. Phys. Chem. A* **2000**, *104*, 12014−12020.

(30) Previous calculations estimated the total resonance energy at 77.2, 102.2, and 107.6 kcal/mol, respectively: (a) Harcourt, R. D. Valence bond studies of oxygen and superoxide: a note on one-electron and two-electron transfer resonances. *J. Phys. Chem.* **1992**, *96*, 7616−7619. (b) Su, P.; Song, L.; Wu, W.; Hiberty, P. C.; Shaik, S. A valence bond study of the dioxygen molecule. *J. Comput. Chem.* **2007**, *28*, 185−197. (c) Danovich, D.; Foroutan-Nejad, C.; Hiberty, P. C.; Shaik, S. Nature of the three-electron bond. *J. Phys. Chem. A* **2018**, *122*, 1873−1885.

(31) In fact, within the context of spin-polarized CDFT, the spin-polarized Fukui functions boil down, in a finite field approximation, to the spin density. See, for example: (a) Galvan, M.; Vela, A.; Gazquez, J. L. Chemical reactivity in spin-polarized density functional theory. *J. Phys. Chem.* **1988**, *92*, 6470−6474. (b) Vargas, R.; Cedillo, A.; Garza, J.; Galvan, M. Reactivity criteria in spin-polarized density functional theory. *Rev. Mod. Quant. Chem.* **2002**, *2*, 936−965.

(32) Ayers, P. W.; Parr, R. G. Variational principles for describing chemical reactions: the Fukui function and chemical hardness revisited. *J. Am. Chem. Soc.* **2000**, *122*, 2010−2018.

https://dx.doi.org/10.1021/jacs.0c02390
J. Am. Chem. Soc. 2020, 142, 10102−10113